Angular dependence of strong field ionization of N$_2$ by time-dependent configuration interaction using density functional theory and the Tamm-Dancoff approximation ⓕ

Paul Hoerner ⓘD, Mi Kyung Lee ⓘD, and H. Bernhard Schlegel ⓘD

COLLECTIONS

Paper published as part of the special topic on Ultrafast Spectroscopy and Diffraction from XUV to X-ray
Note: This paper is part of the JCP special collection on Ultrafast Spectroscopy and Diffraction from XUV to X-ray.

ⓕ   This paper was selected as Featured

View Online   Export Citation   CrossMark

ARTICLES YOU MAY BE INTERESTED IN

Geminal-based configuration interaction
The Journal of Chemical Physics **151**, 051101 (2019); https://doi.org/10.1063/1.5116715

Detecting coherent core-hole wave-packet dynamics in N$_2$ by time- and angle-resolved inner-shell photoelectron spectroscopy
The Journal of Chemical Physics **151**, 054107 (2019); https://doi.org/10.1063/1.5109867

Ultrafast photoelectron spectroscopy of aqueous solutions
The Journal of Chemical Physics **151**, 090901 (2019); https://doi.org/10.1063/1.5098402

Angular dependence of strong field ionization of N_2 by time-dependent configuration interaction using density functional theory and the Tamm-Dancoff approximation

Paul Hoerner, Mi Kyung Lee, and H. Bernhard Schlegel[a]

AFFILIATIONS

Department of Chemistry, Wayne State University, Detroit, Michigan 48202, USA

Note: This paper is part of the JCP special collection on Ultrafast Spectroscopy and Diffraction from XUV to X-ray.
[a]Electronic mail: hbs@chem.wayne.edu

ABSTRACT

The ionization of N_2 serves as an important test case for computational methods for strong field ionization. Because Koopmans's theorem fails for Hartree-Fock calculations of N_2, corrections for electron correlation are needed to obtain the proper ordering of ionization energies of N_2. Lopata and co-workers found that real-time integration of time-dependent Hartree-Fock (rt-TD-HF) gave a ratio for strong field ionization parallel and perpendicular to the molecular axis that was too small compared to experiment, but real-time integration of time-dependent density functional theory (rt-TD-DFT) with an appropriately tuned long-range corrected functional, lc-ωPBE*, was in good agreement with experiment. The present study finds that time-dependent configuration interaction (TDCI) with single excitations based on a Hartree-Fock reference determinant (TD-CIS) has the same problems as rt-TD-HF. These problems can be overcome within the TDCI framework by calculating the excitation energies and transition dipole moments with density functional theory using linear response TD-DFT in the Tamm-Dancoff approximation (TDA) with suitably tuned long-range corrected functionals (TD-TDA). The correct angular dependence of the total ionization rate is obtained with TD-TDA using tuned lc-ωPBE*, lc-BLYP*, and ωB97XD* functionals. Partitioning of the total ionization rate into orbital components confirms that the larger ionization rate perpendicular to the molecular axis found for TD-CIS is due to greater π orbital contributions than those seen in TD-TDA. The use of density functional theory corrects this problem. At higher fields, both the TD-CIS and TD-TDA simulations show an increased ionization rate perpendicular to the molecular axis because of increased ionization from the π orbitals.

Published under license by AIP Publishing. https://doi.org/10.1063/1.5108846

I. INTRODUCTION

Among small molecules, diatomic nitrogen, N_2, has one of the highest ionization potentials (15.58 eV), exceeded only by HF, F_2, and BF_3.[1] Single photon ionization of N_2 requires light in the extreme ultraviolet. Higher intensity UV-Vis light can ionize N_2 by a multiphoton mechanism. If intensities reach the 10^{14} W cm^{-2} range, 800 nm light can ionize N_2 by tunneling ionization and barrier suppression ionization. Ionization rates for laser pulses with these intensities cannot be calculated by the perturbative methods used for linear spectroscopy but must be simulated by solving the

time-dependent Schrödinger equation.[2] The angular dependence of strong field ionization of N_2 has been studied experimentally by a number of groups[3–6] and is an important test case for computational methods for simulating strong field ionization.[7–13]

Various approximate methods based on the single active electron (SAE) approximation have been developed to treat strong field ionization for atoms (e.g., ADK[14]) and have been extended to molecules (e.g., MO-ADK[15,16] and MO-SFA[7,8,17]). More directly, strong field ionization has been simulated by solving the time-dependent Schrödinger equation in the presence of the field of the intense laser pulse. Two approaches that are suitable for

many-electron polyatomic systems in strong fields are time-dependent configuration interaction (TD-CI)[2,18–22] and real-time integration of the time-dependent Hartree-Fock or density functional equations (rt-TD-HF, rt-TD-DFT).[2,23–25]

For most molecules that have been studied by TD-CI or rt-TD-DFT, the angular dependence of strong field ionization is governed to a large extent by the shape of the highest occupied molecular orbital. This is expected from Koopmans's theorem which provides a simple connection between molecular orbitals and ionization. However, it is well known that for some molecules, such as N_2 calculated by Hartree-Fock (HF) theory, Koopmans's theorem fails to give the correct ordering of the ionized states.[26] The correct ordering of the orbital energies and ionization energies can be obtained by density functional theory. Alternatively, accurate ionization energies can be calculated starting from a Hartree-Fock determinant when electron correlation corrections are included by Green's function methods, electron propagator theory (EPT), coupled cluster theory, or multireference configuration interaction.[27–31]

Lopata and co-workers[13] have shown that because of the incorrect ordering of the σ and π orbitals, rt-TD-HF simulations yield the wrong angular dependence for N_2 as the polarization of the laser field is varied from parallel to the molecular axis to perpendicular. However, they found that rt-TD-DFT with an appropriately tuned, long range corrected functional, lc-ωPBE*, gives the correct angular dependence when compared to experimental results. In previous studies, we have used time-dependent configuration interaction with single excitations and a complex absorbing potential, TD-CIS-CAP, to simulate strong field ionization of a variety of molecules.[32–41] Since TD-CIS-CAP is based on a Hartree-Fock reference determinant, it can be expected to have difficulties similar to rt-TD-HF in modeling the angular dependence of strong field ionization of N_2. In the present study, we use linear response TD-DFT in the Tamm-Dancoff approximation (TDA)[42,43] to calculate the energies and matrix elements for singly excited configurations and use these in a TD-CI-CAP approach to simulate the angular dependence of strong field ionization of N_2.

II. COMPUTATIONAL DETAILS

A. TD-CI-CAP and TD-TDA-CAP

In the TD-CI approach, the time dependent wavefunction is obtained by numerically integrating the time-dependent Schrodinger equation (TDSE)

$$|\Psi(t)\rangle = \exp\left[-\frac{i}{\hbar}\int_{t_0}^{t}d\tau\,\hat{H}_{el} - \widehat{\vec{\mu}}\cdot\vec{E}(t) - i\hat{V}^{abs}\right]|\Psi(t_0)\rangle, \quad (1)$$

where $\hat{H}_{el}$ is the field-free electronic Hamiltonian for a given nuclear configuration. Molecular interaction with the laser field is described with the semiclassical dipole approximation where $\widehat{\vec{\mu}}$ is the molecular dipole operator and $\vec{E}(t)$ is the applied electric field. The complex absorbing potential, $-i\hat{V}^{abs}$, models the ionization process by absorbing the wavefunction as an electron is propagated away from the molecule. The time-dependent wavefunction is expanded in the basis of the ground state (HF or DFT) and singly excited configurations (CIS or TDA)

$$|\Psi(t)\rangle = \sum_{I=0}^{N}c_I(t)|\Psi_I\rangle = c_0(t)|\Psi_0\rangle + \sum_{ia}c_{ia}(t)|\Psi_i^a\rangle, \quad (2)$$

where {i, j} refer to occupied orbitals and {a, b} refer to unoccupied orbitals. Numerical integration of the TDSE is carried out with a time step of Δt using the modified-midpoint approximation

$$|\Psi(t+\Delta t)\rangle = \exp\left[-\frac{i}{\hbar}\left(\hat{H}_{el} - \widehat{\vec{\mu}}\cdot\vec{E}\left(t+\frac{\Delta t}{2}\right) - i\hat{V}^{abs}\right)\Delta t\right]|\Psi(t)\rangle. \quad (3)$$

As described previously,[32–35] Trotter-Suzuki factorization of the exponential operator[44] leads to an equation of motion that can be expressed in matrix notation as

$$\mathbf{C}(t+\Delta t) = \exp\left[-\frac{i\Delta t}{2\hbar}\mathbf{H_{el}}\right]\exp\left[-\frac{\Delta t}{2\hbar}\mathbf{V^{abs}}\right]\mathbf{W^T}\exp\left[-\frac{i}{\hbar}E\left(t+\frac{\Delta t}{2}\right)\mathbf{d}\right]$$
$$\times \mathbf{W}\exp\left[-\frac{\Delta t}{2\hbar}\mathbf{V^{abs}}\right]\exp\left[-\frac{i\Delta t}{2\hbar}\mathbf{H_{el}}\right]\mathbf{C}(t). \quad (4)$$

Here, $\mathbf{d}$ is a diagonal matrix of eigenvalues of the transition dipole matrix $\boldsymbol{\mu}$ and $\mathbf{W}$ is a matrix of eigenvectors such that $\mathbf{W}\boldsymbol{\mu}\mathbf{W^T} = \mathbf{d}$.

The TD-CIS-CAP and TD-TDA-CAP simulations were carried out with the stand-alone Fortran90 code used in our previous studies.[32–41] The bond length of N_2, 1.089 Å, was optimized at the PBE0/aug-cc-pVTZ level of theory. Density functional calculations of the singly excited configurations in the linear-response Tamm-Dancoff approximation used the lc-ωPBE*,[45–47] lc-BLYP*,[48–52] and ωB97XD*[53] functionals with a range-separation parameter of ω = 0.5775, 0.580, and 0.490 a_0^{-1}, respectively. Following the approach used by Lopata and co-workers,[13] the range-separation parameters were tuned to minimize the difference between Koopmans's theorem ionization potential and the ΔSCF = $E_{cation} - E_{neutral}$ ionization potential. The absorbing potential for the molecule is equal to the minimum of the values of the atomic absorbing potentials. The atomic potential for each atom is spherical and begins at 3.6 times the van der Waals radius (R_0 = 6.588 Å for N); it rises quadratically and turns over quadratically to 10 hartree at approximately R_0 + 15 Å, as described in an earlier paper.[38] Tests with a $\sin^2$ transition in the absorbing potential[13] instead of a quadratic transition give the same angular shape and differ by less than 2% in the parallel to perpendicular ratio. The integrals needed for the ground and singly excited state energies, transition dipoles, and absorbing potential were computed using a locally modified version of the Gaussian series of programs[54] using the aug-cc-pVTZ basis set[55] with additional diffuse basis functions[38] ("absorbing basis") on each nuclear center (4 s-type gaussian functions with exponents 0.0256, 0.0128, 0.0064, and 0.0032; 4 sets of p-type gaussian functions with exponents 0.0256, 0.0128, 0.0064, and 0.0032; 5 sets of d-type gaussian functions with exponents 0.0512, 0.0256, 0.0128, 0.0064, and 0.0032; 2 sets of f-type gaussian functions with exponents 0.0256, 0.0128). To test this absorbing basis for N_2, we removed the most diffuse spd-type gaussian functions (exponent 0.0032) and found that the ionization yield changed by less than 0.5%. The nitrogen 1s orbitals were frozen, and all singly excited configurations were generated from the remaining orbitals. All configurations with excitation energies less than ca. 20.6 hartree were included in the propagation of the time-dependent wavefunction (1819 states for TD-CIS and 2541 states for TD-TDA). The eigenvalues and eigenvectors needed for the TD-CIS propagation using

Eq. (4) were obtained by standard, in-core matrix diagonalization methods.

To facilitate comparison with the work of Lopata and co-workers,[13] the applied field was taken to be a sinusoidal field with an initial sine squared ramp

$$E(t) = \begin{cases} 0, & t < 0 \\ \sin^2\left(\frac{\pi t}{2\tau}\right)\cos(\omega t), & 0 \leq t \leq \tau, \\ \cos(\omega t), & t > \tau \end{cases} \quad (5)$$

with a frequency of $\omega = 0.057$ a.u., corresponding to a wavelength of 800 nm, and $\tau = 10\pi/\omega$ (i.e., 5 cycles to ramp up to full intensity; see Fig. S4(a) in the supplementary material). An integration time step of 0.05 a.u. (1.2 as) was used for all simulations. Reducing the time step by a factor of 2 changed the norm at the end of the propagation by less than 0.002%.

B. Wavefunction analysis

The instantaneous rate of ionization was taken to be the rate of decrease in the norm squared of the wavefunction, which can be written in terms of the matrix elements of the absorbing potential,

$$\frac{d}{dt}N(t)^2 = \frac{d}{dt}\langle\Psi(t)|\Psi(t)\rangle = -\frac{2}{\hbar}\langle\Psi(t)|\hat{V}^{abs}|\Psi(t)\rangle. \quad (6)$$

In terms of the molecular orbitals and CI coefficients, the instantaneous rate is

$$\frac{d}{dt}N(t)^2 = -\frac{2}{\hbar}\Bigg\{ \sum_i \langle\phi_i|\hat{V}^{abs}|\phi_i\rangle + \sum_{ia} 2\mathbb{R}e\big(c_{ia}^*(t)c_0(t)\big)\langle\phi_a|\hat{V}^{abs}|\phi_i\rangle$$
$$- \sum_{ija} \mathbb{R}e\big(c_{ia}^*(t)c_{ja}(t)\big)\langle\phi_j|\hat{V}^{abs}|\phi_i\rangle$$
$$+ \sum_{iab} \mathbb{R}e\big(c_{ia}^*(t)c_{ib}(t)\big)\langle\phi_a|\hat{V}^{abs}|\phi_b\rangle\Bigg\}. \quad (7)$$

Equation (7) can be further decomposed into contributions to the instantaneous rate from each occupied orbital

$$\left[\frac{d}{dt}N(t)^2\right]_i = -\frac{2}{\hbar}\Bigg\{\langle\phi_i|\hat{V}^{abs}|\phi_i\rangle + \sum_a 2\mathbb{R}e\big(c_{ia}^*(t)c_0(t)\big)\langle\phi_a|\hat{V}^{abs}|\phi_i\rangle$$
$$- \sum_{ja} \mathbb{R}e\big(c_{ia}^*(t)c_{ja}(t)\big)\langle\phi_j|\hat{V}^{abs}|\phi_i\rangle$$
$$+ \sum_{ab} \mathbb{R}e\big(c_{ia}^*(t)c_{ib}(t)\big)\langle\phi_a|\hat{V}^{abs}|\phi_b\rangle\Bigg\}. \quad (8)$$

Instantaneous rates were computed every 50 time steps (60 as). Average ionization rates were calculated by taking the mean of the instantaneous ionization rates from $t = 12$ fs to 20 fs [i.e., after the ramp to full intensity for the laser field in Eq. (5)]. Because there is a small overlap between the occupied orbitals and the absorbing potential, the norm of the wavefunction decreases slowly even in the absence of a field. Similar to the work of Lopata and co-workers,[13] the average ionization rates in a finite field were corrected by subtracting the residual rate obtained from a field-free simulation,

$$\text{Rate} = \left\langle\frac{d}{dt}N(t)^2\right\rangle = \left\langle\frac{d}{dt}N(t)^2_{field}\right\rangle - \left\langle\frac{d}{dt}N(t)^2_{field-free}\right\rangle. \quad (9)$$

III. RESULTS AND DISCUSSION

Computed vertical ionization energies from the ground state of N_2 to the ground and first excited states of N_2^+ are compared with experiment in Table I. Experimentally, the $X^2\Sigma_g^+$ cation is lower than the $A^2\Pi_u$ cation. Ionization energies calculated by Koopmans's theorem and ΔSCF are in the wrong order for Hartree-Fock theory but are in the correct order by density functional theory. Ionization energies calculated by ΔSCF are in the correct order for electron propagator theory (EPT) and coupled cluster theory. The difference in the vertical ionization energies for the lowest two states of N_2^+ is too small for the density functionals considered, too large by EPT, within 0.4 eV of experiment by CISD, and within 0.2 eV of experiment by CCSD(T). Excellent agreement with experiment can be obtained with large MRCI calculations based on a complete active space self-consistent field (CASSCF) wavefunction.[31]

The angular dependence of ionization rates for N_2 calculated by TD-CIS-CAP and TD-TDA-CAP is compared in Figs. 1 and 2 for three different field strengths, $E_{max} = 0.065$ a.u., 0.080 a.u., and 0.095 a.u. (1.48×10^{14}, 2.24×10^{14}, and 3.16×10^{14} W cm^{-2}, respectively). The rates are plotted as the radial distances from the center of the molecule and the angles correspond to the polarization direction of the linearly polarized field given by Eq. (5). Details can be found in Sec. II. The rates for a given field strength are calculated averaging the instantaneous rate, Eq. (7), from $t = 12$ fs to 20 fs and correcting for the residual field-free rate, Eq. (9). For TD-CIS-CAP in Fig. 1(a), there is a prominent bulge perpendicular to the molecular axis for all three intensities. This is because the π orbital is energetically higher than the σ_g orbital in the Hartree-Fock ground state and is more easily ionized. This can be confirmed by partitioning the total ionization rate into components arising from the σ and π orbitals using Eq. (8), as shown in Fig. 1(b). Even at $E_{max} = 0.065$ a.u., the contribution from the π orbital to the ionization rate perpendicular to the molecular axis is greater than the contribution from the σ orbitals (see Fig. S4 in the supplementary material for molecular orbital images).

For the TD-TDA-CAP calculations with the lc-ωPBE* functional shown in Fig. 2, there is little or no bulge perpendicular

TABLE I. Calculated and experimental vertical ionization energies for N_2.[a]

	$X^2\Sigma_g^+$ (N_2^+)		$A^2\Pi_u$ (N_2^+)	
	Koopmans	ΔSCF	Koopmans	ΔSCF
HF	17.34	15.57	17.09	15.74
lc-ωPBE*	16.48	16.44	17.43	17.26
lc-BLYP*	16.56	16.57	17.41	17.31
ωB97XD*	16.62	16.62	17.37	17.32
EPT	15.14		17.41	
CISD	15.99		17.03	
CCSD(T)	15.61		17.21	
Experiment	15.58[b]		~17.0[b]	

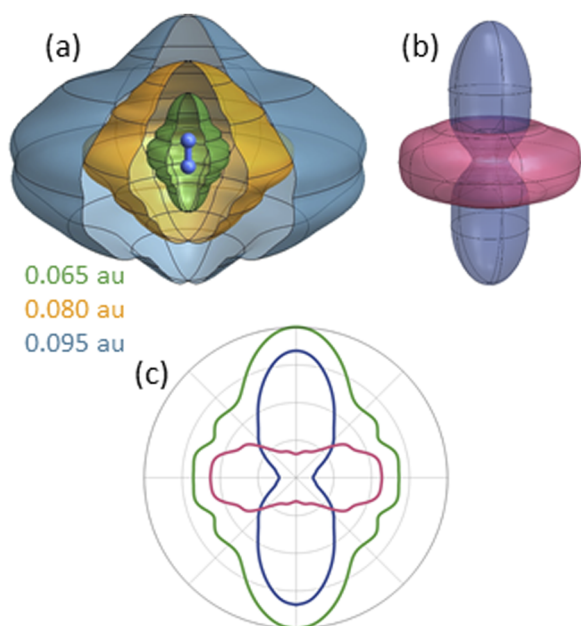[a] In eV, aug-cc-pVTZ used for all calculations.
[b] References 56 and 57.

FIG. 1. (a) Angular dependence of ionization rates calculated by TD-CIS-CAP at field strengths of E_{max} = 0.065 a.u., 0.080 a.u., and 0.095 a.u. (green, yellow, and blue, respectively). The ionization yields are scaled to fit the image and are not to scale relative to each other. (b) and (c) Partitioning of the total ionization rate for E_{max} = 0.065 a.u. into contributions of the σ orbitals (blue) and the π orbitals (pink) to the total (green).
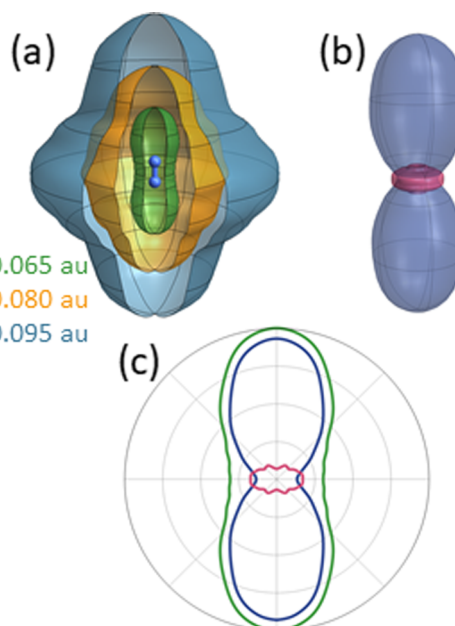

FIG. 2. (a) Angular dependence of ionization rates calculated by TD-TDA-CAP with the lc-ωPBE* functional at field strengths of 0.065 a.u., 0.080 a.u., and 0.095 a.u. (green, yellow, and blue, respectively). The ionization yields are scaled to fit the image and are not to scale relative to each other. (b) and (c) Partitioning of the total ionization rate for E_{max} = 0.065 a.u. into contributions of the σ orbitals (blue) and the π orbitals (pink) to the total (green).

to the molecular axis at lower intensities because the π orbital is lower in energy and harder to ionize than the σ orbital. However, the bulge grows at higher intensities because ionization occurs from both the σ and π orbitals. Similar behavior is seen for the lc-BLYP* and ωB97XD* functionals (see Figs. S1 and S2 in the supplementary material). The evolution of the one-electron difference densities is shown in Figs. S5(b) (Multimedia view) and S5(c) (Multimedia view) in the supplementary material and clearly resembles the shape of the main ionizing molecular orbitals.

The angular dependence of the ionization rates for N_2 obtained from the TD-CIS and TD-TDA simulations is compared to experiment and to rt-TD-HF and rt-TD-DFT calculations by Lopata and co-workers in Fig. 3 for a field strength of 0.065 a.u.. All of the results have been normalized to 1 at Θ = 0° (parallel to the molecular axis). Like rt-TDHF, the TD-CIS-CAP rate is too high at Θ = 90° (perpendicular to the molecular axis) because of too much ionization from the π orbital. When the ground state is calculated with the lc-ωPBE* functional and the excited states are calculated by lr-TD-TDA (i.e., TD-TDA-CAP simulations), the calculated ratio of the ionization rates at Θ = 0° and 90° is in good agreement with experiment[4] and with the rt-TD-DFT calculations by Lopata and co-workers.[13] At intermediate angles, the TD-TDA-CAP ionization rates are somewhat lower than those of experiment and the rt-TDDFT results. Similar behavior is seen for the lc-BLYP* and ωB97XD* functionals (see Fig. S3 in the supplementary material). Qualitatively similar behavior shown in Fig. 3 is seen when the absorbing potential is moved out from 6.588 Å to 11 Å (6 times the van der Waals radius) and when

the absorbing basis is reduced by removing the most diffuse s, p, and d functions with an exponent s of 0.0032. The difference between angle dependence of TD-TDA-CAP and rt-TD-DFT ionization ratios might be attributable to the representation of the time
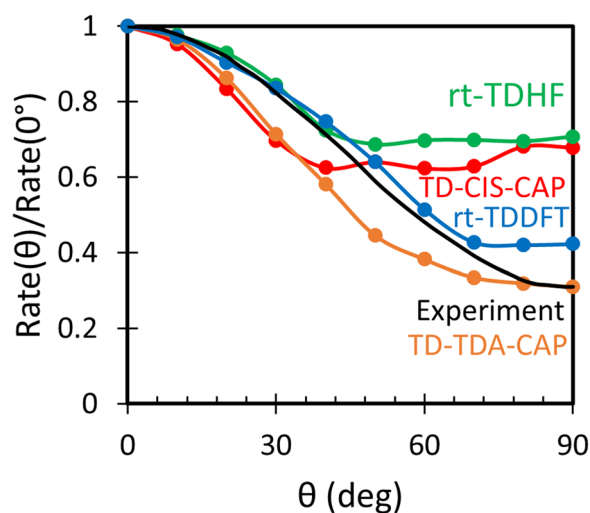

FIG. 3. Angular dependence of ionization rates calculated by TD-CIS-CAP (red) and TD-TDA-CAP (orange) compared with the rt-TDHF (green) and rt-TDDFT (blue) calculations taken from Lopata and co-workers[13] and with experiment (black).[4] The lc-ωPBE* functional was used for the DFT and TDA calculations.
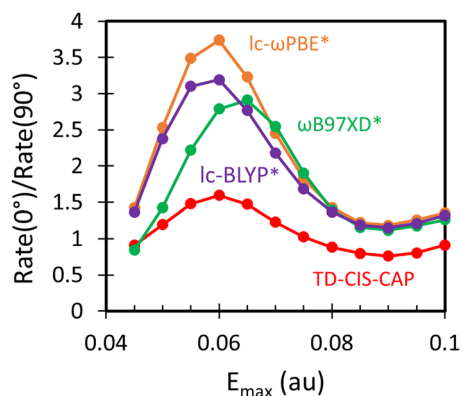
FIG. 4. Ratio of the ionization rate for polarization parallel to the molecular axis to the ionization rate for polarization perpendicular to the molecular axis as a function of field strength calculated with TD-CIS-CAP (red) and TD-TDA-CAP using the lc-ωPBE*, lc-BLYP*, and ωB97XD* functionals (orange, purple, and green, respectively).
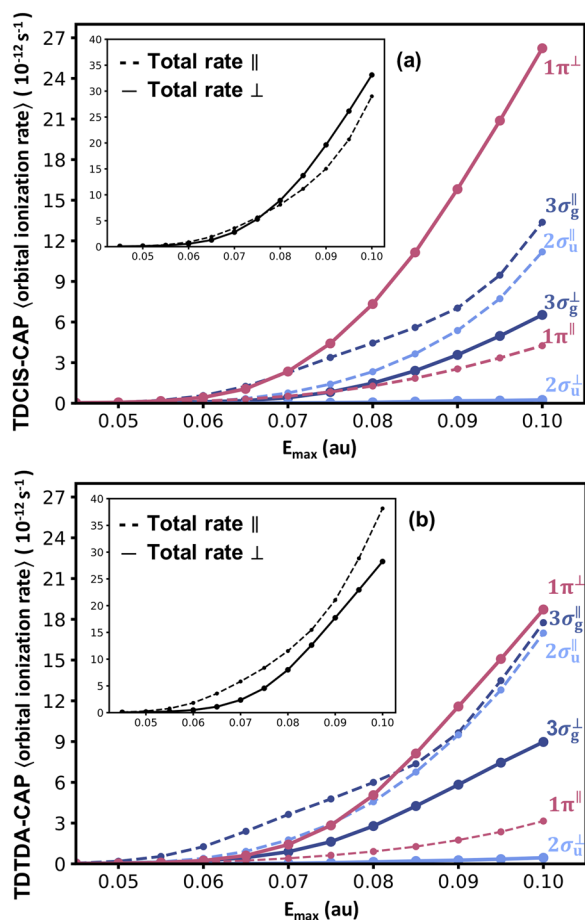

FIG. 5. Contributions to the total ionization rate from the σ orbitals (blue) and π orbitals (pink) for ionization parallel (dashed) and perpendicular (solid) to the molecular axis for (a) TD-CIS-CAP and (b) TD-TDA-CAP. Insets show the total ionization rates parallel (dashed) and perpendicular (solid) to the molecular axis.

dependent wavefunction (linear combination of singly excited field-free configurations vs single determinant of field dependent orbitals) or to the use of the TDA approximation and linear-response TDDFT calculations of the excitation energies.

The ratio of the rates at $\Theta = 0°$ and $90°$ varies with the field strength as shown in Fig. 4. Each of the methods peaks near $E_{max} = 0.06$ a.u., which is a little below the field strength needed for barrier suppression ionization. As the field strength increases, more ionization occurs from the π orbitals in the perpendicular direction, thereby reducing the parallel to perpendicular ionization ratio. Some caution is needed in interpreting the decrease in the ratio for field strengths lower than 0.06 a.u. because the parallel and perpendicular ionization rates become very small and the estimated rates are dominated by the zero-field correction [Eq. (9)].

Contributions of the individual orbitals to the total ionization rates can be calculated by Eq. (8). Figure 5 shows the contributions to the ionization rates parallel and perpendicular to the molecular axis for TD-CIS-CAP and TD-TDA-CAP simulations as a function of field strength. In both simulations, as expected for the parallel direction, the σ orbitals dominate the ionization rate. Surprisingly, the $2\sigma_u$ orbital contribution is nearly as large as the higher lying $3\sigma_g$ orbital for higher field strengths. For the perpendicular direction, ionization from 1π orbitals dominates. The contribution from the $3\sigma_g$ orbital is about half as much as from the 1π orbital, but the contribution from the $2\sigma_u$ orbital is very small because it has a node perpendicular to the molecular axis. When all of the components are added together, the parallel rate is larger than the perpendicular rate for TD-TDA-CAP because of a larger parallel to perpendicular ratio for the $3\sigma_g$ and $2\sigma_u$ contributions and a smaller ratio for the 1π contributions.

IV. SUMMARY

The experimentally determined angular dependence of strong field ionization of N_2 serves as an important test case for computational methods for strong field ionization. Lopata and co-workers found that rt-TD-HF strong field simulations yielded a ratio for ionization parallel and perpendicular to the molecular axis that was too small compared to experiment. This was traced to the well-known failure of Koopmans's theorem to give the correct order of ionized states of N_2 when calculated by Hartree-Fock theory. They showed that an appropriately tuned long-range corrected functional, lc-ωPBE*, gives the correct ordering of the N_2 cation states and rt-TD-DFT simulations with this functional match the experimentally determined angular dependence of strong field ionization. In the present study, we show that TD-CIS-CAP simulations of strong field ionization of N_2 have the same problems as rt-TD-HF simulations, resulting in a bulge in the ionization rate perpendicular to the molecular axis. We demonstrate that these problems can be overcome within the TD-CI framework by calculating the excitation energies and transition dipole moments with density functional theory using linear response TD-DFT in the Tamm-Dancoff approximation with suitably tuned long-range corrected functionals (TD-TDA-CAP). Partitioning of the angular dependence of the total ionization rate into orbital contributions demonstrates that incorrect ordering of the σ and π orbital energies at the Hartree-Fock level of theory is responsible for the higher than expected ionization rate perpendicular to the molecular axis. The proper ordering of the orbital

energies with density functional theory corrects this problem. Nevertheless, when the field strength is increased, contributions from the π orbital increase and ionization perpendicular to the molecular axis increases relative to ionization parallel to the molecular axis. Both the TD-CIS-CAP and TD-TDA-CAP simulations show a bulge in the ionization rate perpendicular to the molecular axis at high fields. However, ionization parallel to the molecular axis remains greater than ionization perpendicular to the axis for TD-TDA-CAP calculations.

SUPPLEMENTARY MATERIAL

See supplementary material for (S1) angular dependence of ionization rates and orbital contributions computed with the lc-BLYP* functional, (S2) angular dependence of ionization rates and orbital contributions computed with the ωB97XD* functional, (S3) normalized ionization rates as a function of Θ computed with lc-BLYP* and ωB97XD*, (S4) molecular orbitals and energies computed with HF and lc-ωPBE*, and (S5) applied field in accordance with Eq. (5) and difference densities at t = 15.72 fs for field polarized parallel and perpendicular to the molecular axis. Evolution of the difference densities is shown in Figs. S5(b) (Multimedia view) and S5(c) (Multimedia view).

REFERENCES

[1] See https://webbook.nist.gov/chemistry/ for NIST Chemistry WebBook.

[2] M. Nisoli, P. Decleva, F. Calegari, A. Palacios, and F. Martin, "Attosecond electron dynamics in molecules," Chem. Rev. **117**, 10760 (2017).

[3] I. V. Litvinyuk, K. F. Lee, P. W. Dooley, D. M. Rayner, D. M. Villeneuve, and P. B. Corkum, "Alignment-dependent strong field ionization of molecules," Phys. Rev. Lett. **90**, 233003 (2003).

[4] D. Pavicic, K. F. Lee, D. M. Rayner, P. B. Corkum, and D. M. Villeneuve, "Direct measurement of the angular dependence of ionization for N_2, O_2, and CO_2 in intense laser fields," Phys. Rev. Lett. **98**, 243001 (2007).

[5] I. Thomann, R. Lock, V. Sharma, E. Gagnon, S. T. Pratt, H. C. Kapteyn, M. M. Murnane, and W. Li, "Direct measurement of the angular dependence of the single-photon ionization of aligned N_2 and CO_2," J. Phys. Chem. A **112**, 9382 (2008).

[6] P. den Hoff, I. Znakovskaya, S. Zherebtsov, M. F. Kling, and R. de Vivie-Riedle, "Effects of multi orbital contributions in the angular-dependent ionization of molecules in intense few-cycle laser pulses," Appl. Phys. B: Lasers Opt. **98**, 659 (2010).

[7] A. Jaron-Becker, A. Becker, and F. H. M. Faisal, "Ionization of N_2, O_2, and linear carbon clusters in a strong laser pulse," Phys. Rev. A **69**, 023410 (2004).

[8] T. K. Kjeldsen and L. B. Madsen, "Strong-field ionization of N_2: Length and velocity gauge strong-field approximation and tunnelling theory," J. Phys. B: At., Mol. Opt. Phys. **37**, 2033 (2004).

[9] V. I. Usachenko and S. I. Chu, "Strong-field ionization of laser-irradiated light homonuclear diatomic molecules: A generalized strong-field approximation-linear combination of atomic orbitals model," Phys. Rev. A **71**, 063410 (2005).

[10] S. F. Zhao, L. Liu, and X. X. Zhou, "Multiphoton and tunneling ionization probability of atoms and molecules in an intense laser field," Opt. Commun. **313**, 74 (2014).

[11] V. P. Majety and A. Scrinzi, "Dynamic exchange in the strong field ionization of molecules," Phys. Rev. Lett. **115**, 103002 (2015).

[12] V. P. Majety and A. Scrinzi, "Static field ionization rates for multi-electron atoms and small molecules," J. Phys. B: At., Mol. Opt. Phys. **48**, 245603 (2015).

[13] A. Sissay, P. Abanador, F. Mauger, M. Gaarde, K. J. Schafer, and K. Lopata, "Angle-dependent strong-field molecular ionization rates with tuned range-separated time-dependent density functional theory," J. Chem. Phys. **145**, 094105 (2016).

[14] M. V. Ammosov, N. B. Delone, and V. P. Krainov, "Tunnel ionization of complex atoms and of atomic ions in an alternating electromagnetic field," Sov. Phys. JETP **64**, 1191 (1986).

[15] J. Muth-Bohm, A. Becker, and F. H. M. Faisal, "Suppressed molecular ionization for a class of diatomics in intense femtosecond laser fields," Phys. Rev. Lett. **85**, 2280 (2000).

[16] X. M. Tong, Z. X. Zhao, and C. D. Lin, "Theory of molecular tunneling ionization," Phys. Rev. A **66**, 033402 (2002).

[17] A. Jaron-Becker, A. Becker, and F. H. M. Faisal, "Dependence of strong-field photoelectron angular distributions on molecular orientation," J. Phys. B: At., Mol. Opt. Phys. **36**, L375 (2003).

[18] N. Rohringer, A. Gordon, and R. Santra, "Configuration-interaction-based time-dependent orbital approach for ab initio treatment of electronic dynamics in a strong optical laser field," Phys. Rev. A **74**, 043420 (2006).

[19] H. B. Schlegel, S. M. Smith, and X. Li, "Electronic optical response of molecules in intense fields: Comparison of TD-HF, TD-CIS, and TD-CIS(D) approaches," J. Chem. Phys. **126**, 244110 (2007).

[20] L. Greenman, P. J. Ho, S. Pabst, E. Kamarchik, D. A. Mazziotti, and R. Santra, "Implementation of the time-dependent configuration-interaction singles method for atomic strong-field processes," Phys. Rev. A **82**, 023406 (2010).

[21] J. A. Sonk and H. B. Schlegel, "TD-CI simulation of the electronic optical response of molecules in intense fields II: Comparison of DFT functionals and EOM-CCSD," J. Phys. Chem. A **115**, 11832 (2011).

[22] D. Toffoli and P. Decleva, "A multichannel least-squares B-spline approach to molecular photoionization: Theory, implementation, and applications within the configuration-interaction singles approximation," J. Chem. Theory Comput. **12**, 4996 (2016).

[23] K. Yabana and G. F. Bertsch, "Time-dependent local-density approximation in real time," Phys. Rev. B **54**, 4484 (1996).

[24] A. Castro, M. A. L. Marques, and A. Rubio, "Propagators for the time-dependent Kohn-Sham equations," J. Chem. Phys. **121**, 3425 (2004).

[25] M. R. Provorse and C. M. Isborn, "Electron dynamics with real-time time-dependent density functional theory," Int. J. Quantum Chem. **116**, 739 (2016).

[26] A. Szabo and N. S. Ostlund, *Modern Quantum Chemistry* (McGraw-Hill, New York, 1989).

[27] L. S. Cederbaum and W. V. Niessen, "Ionization-potentials of N_2 by a Greens function approach," J. Chem. Phys. **62**, 3824 (1975).

[28] E. W. Thulstrup and A. Andersen, "Configuration interaction studies of bound, low-lying states of $N_2(-)$, N_2, $N_2(+)$ and $N_2(2+)$," J. Phys. B: At., Mol. Opt. Phys. **8**, 965 (1975).

[29] D. Spelsberg and W. Meyer, "Dipole-allowed excited states of N_2: Potential energy curves, vibrational analysis, and absorption intensities," J. Chem. Phys. **115**, 6438 (2001).

[30] X. Z. Li and J. Paldus, "Symmetry breaking in spin-restricted Hartree-Fock solutions: The case of the C_2 molecule and the $N_2(+)$ and $F_2(+)$ cations," Phys. Chem. Chem. Phys. **11**, 5281 (2009).

[31] D. Shi, W. Xing, J. Sun, Z. Zhu, and Y. Liu, "Spectroscopic constants and molecular properties of $X^2\Sigma(+)(g)$, $A^2\Pi(u)$, $B^2\Sigma(+)(u)$ and $D^2\Pi(g)$ electronic states of the $N_2(+)$ ion," Comput. Theor. Chem. **966**, 44 (2011).

[32] P. Krause and H. B. Schlegel, "Strong-field ionization rates of linear polyenes simulated with time-dependent configuration interaction with an absorbing potential," J. Chem. Phys. **141**, 174104 (2014).

[33] P. Krause, J. A. Sonk, and H. B. Schlegel, "Strong field ionization rates simulated with time-dependent configuration interaction and an absorbing potential," J. Chem. Phys. **140**, 174113 (2014).

[34] P. Krause and H. B. Schlegel, "Angle-dependent ionization of hydrides AH_n calculated by time-dependent configuration interaction with an absorbing potential," J. Phys. Chem. A **119**, 10212 (2015).

[35] P. Krause and H. B. Schlegel, "Angle-dependent ionization of small molecules by time-dependent configuration interaction and an absorbing potential," J. Phys. Chem. Lett. **6**, 2140 (2015).

[36] Q. Liao, W. Li, and H. B. Schlegel, "Angle-dependent strong-field ionization of triple bonded systems calculated by time-dependent configuration interaction with an absorbing potential," Can. J. Chem. **94**, 989 (2016).

[37] P. Hoerner and H. B. Schlegel, "Angular dependence of ionization by circularly polarized light calculated with time-dependent configuration interaction with an absorbing potential," J. Phys. Chem. A **121**, 1336 (2017).

[38] P. Hoerner and H. B. Schlegel, "Angular dependence of ionization of CH_3X using time-dependent configuration interaction with an absorbing potential," J. Phys. Chem. A **121**, 5940 (2017).

[39] P. Hoerner and H. B. Schlegel, "Angular dependence of strong field ionization of haloacetylenes, HCCX (X = F, Cl, Br, I) using time-dependent configuration interaction with an absorbing potential," J. Phys. Chem. C **122**, 13751 (2018).

[40] A. H. Winney, S. K. Lee, Y. F. Lin, Q. Liao, P. Adhikari, G. Basnayake, H. B. Schlegel, and W. Li, "Attosecond electron correlation dynamics in double ionization of benzene probed with two-electron angular streaking," Phys. Rev. Lett. **119**, 123201 (2017).

[41] A. H. Winney, G. Basnayake, D. A. Debrah, Y. F. Lin, S. K. Lee, P. Hoerner, C. Liao, H. B. Schlegel, and W. Li, "Disentangling strong-field multielectron dynamics with angular streaking," J. Phys. Chem. Lett. **9**, 2539 (2018).

[42] S. Hirata and M. Head-Gordon, "Time-dependent density functional theory within the Tamm-Dancoff approximation," Chem. Phys. Lett. **314**, 291 (1999).

[43] A. Dreuw and M. Head-Gordon, "Single-reference *ab initio* methods for the calculation of excited states of large molecules," Chem. Rev. **105**, 4009 (2005).

[44] M. Suzuki, "General decomposition-theory of ordered exponentials," Proc. Jpn. Acad., Ser. B **69**, 161 (1993).

[45] J. P. Perdew, K. Burke, and M. Ernzerhof, "Generalized gradient approximation made simple," Phys. Rev. Lett. **77**, 3865 (1996).

[46] J. P. Perdew, K. Burke, and M. Ernzerhof, "Generalized gradient approximation made simple [Phys. Rev. Lett. 77, 3865 (1996)]," Phys. Rev. Lett. **78**, 1396 (1997).

[47] O. A. Vydrov and G. E. Scuseria, "Assessment of a long-range corrected hybrid functional," J. Chem. Phys. **125**, 234109 (2006).

[48] A. D. Becke, "Density-functional exchange-energy approximation with correct asymptotic behavior," Phys. Rev. A **38**, 3098 (1988).

[49] A. D. Becke, "Density-functional thermochemistry. III. The role of exact exchange," J. Chem. Phys. **98**, 5648 (1993).

[50] C. Lee, W. Yang, and R. G. Parr, "Development of the Colle-Salvetti correlation-energy formula into a functional of the electron density," Phys. Rev. B **37**, 785 (1988).

[51] P. Stephens, F. Devlin, C. Chabalowski, and M. J. Frisch, "*Ab initio* calculation of vibrational absorption and circular dichroism spectra using density functional force fields," J. Phys. Chem. **98**, 11623 (1994).

[52] H. Iikura, T. Tsuneda, T. Yanai, and K. Hirao, "A long-range correction scheme for generalized-gradient-approximation exchange functionals," J. Chem. Phys. **115**, 3540 (2001).

[53] J.-D. Chai and M. Head-Gordon, "Long-range corrected hybrid density functionals with damped atom–atom dispersion corrections," Phys. Chem. Chem. Phys. **10**, 6615 (2008).

[54] M. J. Frisch, G. W. Trucks, H. B. Schlegel, G. E. Scuseria *et al.*, GAUSSIAN Development Version, Revision I.09, Gaussian, Inc., Wallingford, CT, 2010.

[55] T. H. Dunning, "Gaussian-basis sets for use in correlated molecular calculations. 1. The atoms boron through neon and hydrogen," J. Chem. Phys. **90**, 1007 (1989).

[56] K. P. Huber and G. Herzberg, *Molecular Spectra and Molecular Structure*, Constants of Diatomic Molecules Vol. 4 (Van Nostrand Reinhold, New York, 1979).

[57] J. L. Gardner and J. A. R. Samson, "Photoion and photoelectron spectroscopy of CO and N_2," J. Chem. Phys. **62**, 1447 (1975).